Catalytic and Charge Transfer Properties of Transition Metal Dichalcogenides Arising from Electrochemical Pretreatment

Xinyi Chia,[†] Adriano Ambrosi,[†] Zdenek Sofer,[‡] Jan Luxa,[‡] and Martin Pumera*[,†]

[†]Division of Chemistry & Biological Chemistry, School of Physical and Mathematical Sciences, Nanyang Technological University, 637371 Singapore and
[‡]Department of Inorganic Chemistry, University of Chemistry and Technology Prague, Technicka 5, 166 28, Prague 6, Czech Republic

ABSTRACT

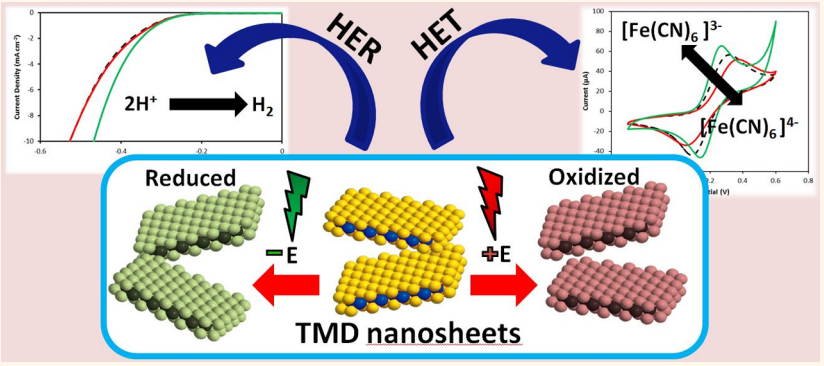

Layered transition metal dichalcogenides (TMDs) have been the center of attention in the scientific community due to their properties that can be tapped on for applications in electrochemistry and hydrogen evolution reaction (HER) catalysis. We report on the effect of electrochemical treatment of exfoliated MoS_2, WS_2, $MoSe_2$ and WSe_2 nanosheets toward the goal of activating the electrochemical and HER catalytic properties of the TMDs. In particular, electrochemical activation of the heterogeneous electron transfer (HET) abilities of MoS_2, $MoSe_2$ and WSe_2 is achieved *via* reductive treatments at identified reductive potentials based on their respective inherent electrochemistry. Comparing all TMDs, the charge transfer activation is most accentuated in $MoSe_2$ and can be concluded that Mo metal and Se chalcogen type are more susceptible to electrochemical activation than W metal and S chalcogen type. With regards to the HER, we show that while MoS_2 displayed enhanced performance when subjected to electrochemical reduction, WS_2 fared worse upon oxidation. On the other hand, the HER performance of $MoSe_2$ and WSe_2 is independent of electrochemical redox treatment. We can conclude therefore that for the HER, S-containing TMDs are more responsive to redox treatment than compounds with the Se chalcogen. Our findings are beneficial toward understanding the electrochemistry of TMDs and the extent to which activation by electrochemical means is effective. In turn, when such knowledge is administered aptly, it will be promising for electrochemical uses.

KEYWORDS: transition metal chalcogenides · two-dimensional materials · activation · electrochemistry · hydrogen evolution

The advent of graphene research unearths a host of its remarkable properties in optical, electronic and mechanical aspects,[1,2] and spurred on studies into other two-dimensional (2D) materials. Amidst the 2D materials, the realms of transition metal dichalcogenides (TMDs) have been pursued with great fervor. Akin to graphite, TMDs are layered structures. Each layer consists of a transition metal (*e.g.*, Mo, W) atom sandwiched between two hexagonal lattices of chalcogen (*e.g.*, S, Se) atoms. Within the layers, the atoms are held by strong covalent bonds, whereas adjacent layers are weakly bonded by van der Waals' forces.

In the past, bulk forms of TMDs have been extensively studied for their use as solid state lubricants.[3] At present, TMDs in ultrathin layers is all the rage in the scientific community. Contemporary literature has elucidated promising layer-dependent properties

* Address correspondence to pumera.research@gmail.com.

Received for review January 23, 2015 and accepted April 13, 2015.

Published online April 20, 2015
10.1021/acsnano.5b00501

of TMDs. One of these properties is the transition in semiconducting nature of TMDs from having an indirect to a direct band gap[4,5] when the bulk form is exfoliated into single layers as a result of quantum confinement effects.[6] Bulk MoS_2, for example, possesses an indirect band gap of 1.2 eV,[7] but once exfoliated into MoS_2 nanosheets, it affords a direct band gap of 1.9 eV[8] giving rise to novel photoluminescence[9] and electronic properties.[10] Another important feature is the massive surface area created when the bulk is thinned down into layers. Such large surface area in exfoliated TMD nanosheets carries high density of edges which are potential active sites for electrochemical applications in sensing and energy production, in particular for hydrogen evolution reaction (HER).[11,12]

The allure of hydrogen energy boils down to its high energy density[13] and clean byproduct. Hence, hydrogen may be the panacea to the global concern of rising carbon emissions due to the burning of hydrocarbon to produce energy. Generating hydrogen on a large-scale in a sustainable manner requires a competent catalyst made from materials that are abundant. Platinum is widely established as the best HER catalyst in terms of HER efficiency;[14,15] however, its major drawback is its low abundance. Existing in relatively high natural abundance compared to platinum, exfoliated TMD nanosheets have generated a great deal of attention as potential electrocatalysts for HER.[16] The HER activity of TMD nanosheets stems from their edges while their basal planes are deemed inert.[17−19] Efforts are underway to develop TMDs with optimized HER abilities comparable to platinum such as by increasing the number of active sites,[20,21] improving electrical conductivity[11,22] and enhancing the catalytic capacity of the active sites.[23−27]

Our previous work[28] reported on the electrochemical tuning of the charge transfer kinetics and HER catalytic properties of bulk and exfoliated MoS_2 nanosheets. Electrochemically reduced MoS_2 materials achieved an enhancement in charge transfer kinetics and improved HER. Most intriguing is that the effects of electrochemical tuning were more prominent in exfoliated MoS_2 nanosheets than its bulk form. Inspired by these findings, we extend this present study beyond exfoliated MoS_2 nanosheets, into other layered TMD materials to investigate the impact of electrochemical anodization or cathodization on their properties. Herein, we present a fundamental study on the electrochemistry of exfoliated MoS_2, WS_2, $MoSe_2$ and WSe_2 nanosheets and examine the effect of an oxidative or reductive electrochemical treatment on their electrochemical and HER catalytic behavior. Characterization of the TMD materials using X-ray photoelectron spectroscopy (XPS), Raman spectroscopy and high resolution transmission electron microscopy (HR-TEM) were also performed to compare the surface and structural morphologies of the exfoliated TMDs before and after electrochemical treatment. It is also of interest to determine how the type of metal and chalcogen govern the electrochemical and catalytic performance.

RESULTS AND DISCUSSION

We conducted a study on the electrochemical behavior of exfoliated transition metal dichalcogenides (TMDs) comprising the exfoliated MoS_2, $MoSe_2$, WS_2 and WSe_2 nanosheets. Cyclic voltammetry measurements on the exfoliated TMD materials were performed over a potential window from −1.8 to 1.8 V in phosphate buffered saline (PBS) as electrolyte at pH 7.0. These TMD materials were electrochemically oxidized or reduced in an attempt to alter the electrochemical and catalytic properties of materials, in terms of heterogeneous electron transfer (HET) rates, which is studied in the presence of inner- and outer-sphere classical redox probes which are respectively $[Fe(CN)_6]^{4-/3-}$ and $[Ru(NH_3)_6]^{2+/3+}$, and as electrocatalysts for hydrogen evolution reaction (HER).

Inherent Electrochemistry of Exfoliated Transition Metal Dichacolgenide (TMD) Nanosheets. At present, fundamental knowledge on the inherent electrochemistry of exfoliated MoS_2, WS_2, $MoSe_2$ and WSe_2 nanosheets is inadequate.[29] We first explore this by conducting cyclic voltammetry in two scan directions: anodic and cathodic. The acquired voltammetric profiles of the anodic and cathodic scans reveal information about the electroactive surface moieties of the TMD materials. Three consecutive scans were recorded to determine the nature of electrochemical processes in the TMD nanosheets. Figure 1 illustrates the cyclic voltammograms of anodic and cathodic scans of exfoliated MoS_2, WS_2, $MoSe_2$, and WSe_2 nanosheets at pH 7.0. We also performed cyclic voltammetry under similar conditions for MoO_2, MoO_3, WO_2 and WO_3 to identify the possible electrochemical processes occurring in the exfoliated TMDs and the voltammograms of Mo and W oxides are captured in Figure S1 (Supporting Information, SI). It is important to highlight that all potentials stated in this paper are *versus* Ag/AgCl, with the exception of HER where they are stated *versus* RHE.

The redox peaks are distinctive to various TMD materials. They arise from the type and number of electroactive groups present on the surface of the TMDs. The first scan of exfoliated MoS_2 nanosheets in the anodic direction resulted in an oxidation peak at *ca.* 0.9 V while the first scan toward the cathodic potential showed a shoulder reduction peak at *ca.* −1.2 V and a mild oxidation peak at *ca.* 0.8 V as seen in Figure 1a and 1b. The absence of a reduction peak during the anodic scan indicates that an initial oxidation renders the electroactive moieties on exfoliated MoS_2 nanosheets less susceptible to reduction. During the first anodic scan, exfoliated WS_2 nanosheets possess an oxidation peak at *ca.* 1.2 V of significant intensity at 1000 μA and a shoulder reduction peak at *ca.* −1.6 V. When first swept toward the cathodic direction in Figure 1d, two

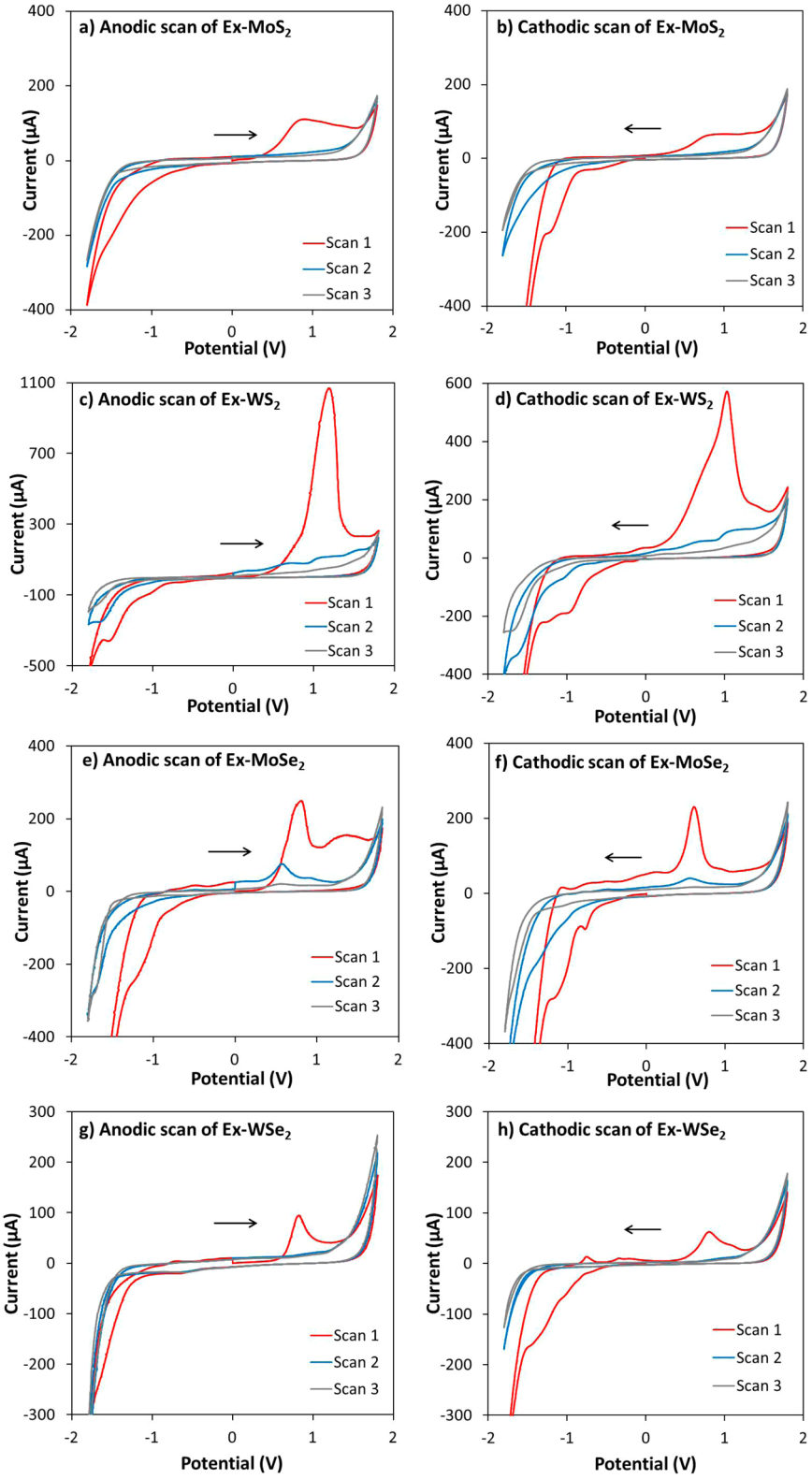

Figure 1. Cyclic voltammograms of (a) exfoliated MoS_2 nanosheets during anodic scan and (b) cathodic scan, (c) exfoliated WS_2 nanosheets during anodic scan and (d) cathodic scan, (e) exfoliated $MoSe_2$ nanosheets during anodic scan and (f) cathodic scan, (g) exfoliated WSe_2 nanosheets during anodic scan and (h) cathodic scan. Conditions: background electrolyte, PBS (50 mM), pH 7.0; scan rate, 100 mV s^{-1}; all measurements are performed relative to the Ag/AgCl reference electrode.

inconspicuous reduction peaks emerged at *ca.* −1.0 V, followed by *ca.* −1.3 V and an apparent oxidation peak appeared at *ca.* 1.0 V of current intensity 570 μA, at nearly half the current intensity of the anodic scan. The vast disparity between the oxidation current intensities in anodic and cathodic scans points to the possibility

that the initial cathodic scan significantly depletes the number of oxidizable groups on the surface of exfoliated WS_2 nanosheets. Another inference drawn from the immense current intensities of the oxidation peaks relative to the reduction peaks of exfoliated WS_2 nanosheets in anodic and cathodic scans depicts majority of the surface groups are oxidizable moieties. As illustrated in Figure 1e, two distinct oxidation peaks materialized as a sharp peak at *ca.* 0.8 V and another as a broad peak at a higher potential of *ca.* 1.3 V in the first anodic scan of exfoliated $MoSe_2$ nanosheets. The oxidation peak at *ca.* 0.8 V is deemed the main oxidation peak because it displayed higher current intensity than the other oxidation peak at *ca.* 1.3 V. The presence of two oxidation peaks indicates 2 different oxidative processes occurring on the surface of exfoliated $MoSe_2$ nanosheets. There is also a faint reduction peak at −1.2 V. Conversely, two shoulder reduction peaks appeared at *ca.* −0.7 V and *ca.* −1.1 V while a sharp oxidation peak at a potential of *ca.* 0.6 V during the first cathodic scan. An initial reduction is necessary for two reductive processes to occur in exfoliated $MoSe_2$ nanosheets. In exfoliated WSe_2 nanosheets, initial anodic and cathodic scans revealed a modest oxidation peak at the same potential at *ca.* 0.7 V. While no reduction peaks were visible in the anodic scan, a reduction peak appeared in the cathodic scan at a potential of *ca.* −1.4 V. Thus, it is deduced that the preceding anodic scan lowers the activity of reducible groups on the exfoliated WSe_2 nanosheets.

Evidence in Figure S1 (SI) showcases the inherent electrochemistry of the Mo and W oxides and provides insights into the possible electrochemical processes responsible for the observations in TMDs. The oxidation peak of MoO_2 at *ca.* 0.9 V coincides with the anodic peaks in Mo chalcogenides. Similarly, the reduction peak of MoO_3 at *ca.* −1.0 V lies close to the more negative cathodic peaks in Mo chalcogenides. Hence, this affirms the oxidation of Mo metal center in Mo chalcogenides to 4+ to 6+ states at *ca.* 0.9 V and the reduction from 6+ to 4+ states at *ca.* −1.0 V. Unaccounted for redox peaks at *ca.* −0.8 V in MoS_2 and *ca.* 1.3 V in $MoSe_2$ may stem from the redox behavior of the chalcogens (S, Se). Reduction of WO_3 occurs at *ca.* −0.8 and −1.4 V as seen in Figure S1h (SI) concurs with the 2 cathodic peaks in WS_2 and the peak at −1.4 V coincides with the single cathodic peak in WSe_2. Oxidation of WO_2 manifests as a low and broad peak unlike the sharp anodic peaks in W chalcogenides. Besides the participation of 4+ and 6+ oxidation states in W, the disparity in the peak shape could be a result of the redox processes in the chalcogens.

The electrochemical processes corresponding to the characteristic oxidations and reductions are, to a large extent, chemically irreversible. As supported by the anodic and cathodic scans of exfoliated MoS_2 nanosheets in Figure 1a and 1b, the visible peaks observed during the initial oxidative and reductive sweeps vanished in the subsequent scans. This observation also applies to exfoliated WSe_2 nanosheets wherein the initially distinct redox peaks in the anodic and cathodic sweeps, illustrated in Figure 1g and 1h, virtually disappeared from subsequent scans. Clearly, redox processes occurring on exfoliated MoS_2 and WSe_2 nanosheets proceed to completion in the first scan and are regarded as irreversible. Unlike exfoliated MoS_2 and WSe_2 nanosheets, which exhibited immediate decline of the current intensity of their redox peaks after the first scan, peak heights of exfoliated WS_2 and $MoSe_2$ nanosheets diminish gradually. The reduction peaks of exfoliated WS_2 nanosheets, during both initial anodic and cathodic scans, weakened in current intensity by at least 70% in the second scans and a marked decrease in the third scans. Analogous to exfoliated WS_2 nanosheets, reduction peaks of exfoliated $MoSe_2$ nanosheets exhibited decreasing peak current intensities in subsequent scans except for the reduction peak at *ca.* −0.7 V in the cathodic scan that became unnoticeable after the first scan. It may be explained that the reducible moieties on exfoliated $MoSe_2$ nanosheets were thoroughly consumed during reduction at *ca.* −0.7 V in the initial scan. Likewise, the oxidation peak of the anodic scan at *ca.* 1.3 V disappeared in subsequent scans; a possibility is that the oxidizable moieties on exfoliated $MoSe_2$ nanosheets at *ca.* 1.3 V were depleted by an irreversible oxidation during the initial scan. The main oxidation peak occurring at *ca.* 0.8 V waned in current intensity by 70% and shifted to a lower potential at *ca.* 0.5 V in the second scan. The shift in potential is likely ascribed to the reduction process that added moieties prone to oxidation so that oxidation is enabled at earlier potentials. The potential shift was not observed when exfoliated $MoSe_2$ nanosheets were swept in the cathodic direction first. The current intensity of the sharp oxidation peak at *ca.* 0.6 V plunged by 80% in the second scan demonstrating that most of the moieties were oxidized in the first scan and few oxidizable moieties were available thereafter. It is also of interest to note that the anodic scan of exfoliated WS_2 nanosheets showcased a single intense oxidation peak at *ca.* 1.2 V in the first scan disintegrated into three minor oxidation peaks at potentials of *ca.* 0.6 V, 1.1 and 1.6 V subsequently. Therefore, the initial reduction of the moieties on exfoliated WS_2 nanosheets during the anodic scan is a prelude to the 3 separate oxidation processes that arise during the second scan. A similar trend is also noted during the cathodic scan with two minor oxidation peaks during the second scan at potentials of *ca.* 0.7 and 1.0 V wherein *ca.* 1.0 V coincides with the single oxidation peak in the initial scan. In this instance, the presence of two mild oxidation peaks during the cathodic scan sheds light on the massive oxidation peak, which is deduced to be a merger of the 2 oxidative

processes also existing in the first cathodic scan. On speculation, the oxidation process at *ca.* 1.0 V involved more electroactive moieties compared to *ca.* 0.7 V. Thus, oxidation peak at *ca.* 0.7 V in the initial cathodic scan was masked by the high current intensity generated by the oxidation process at *ca.* 1.0 V. The two processes become distinguishable during the second scan because the bulk of electroactive moieties on exfoliated WS_2 nanosheets have been oxidized in the initial scan and the remaining oxidizable moieties at these potentials are in comparable quantities.

On the basis of these findings, the unique oxidative and reductive peaks are inherent to different TMD materials and characteristic of their innate electrochemistry. However, exact mechanisms behind the inherent redox reactions of the TMD nanosheets have not been unveiled and require in-depth studies. We may postulate that the oxidation and reduction processes of exfoliated MoS_2, WS_2, $MoSe_2$ and WSe_2 nanosheets are largely chemically irreversible. In particular, oxidation of exfoliated MoS_2 and WSe_2 nanosheets proceeded to completion as their respective electroactive moieties were not rereduced in subsequent scans. Similarly, the reduction of exfoliated MoS_2 and WSe_2 nanosheets were fully reduced in the first scan and did not reoxidize in subsequent scans.

Effect of Electrochemical Treatment on Exfoliated Transition Metal Dichalcogenide (TMD) Nanosheets. Earlier, we studied the inherent electrochemistry of exfoliated MoS_2, WS_2, $MoSe_2$ and WSe_2 nanosheets and identified characteristic oxidation and reduction peaks of the TMD materials. For each of the TMD material, we determine a suitable oxidation and reduction potential that lie marginally beyond their characteristic redox potentials for treatment as described in the previous section. The oxidation and reduction treatment potentials are determined to be 1.1 and −1.3 V for exfoliated MoS_2 nanosheets, 1.2 and −1.6 V for exfoliated WS_2 nanosheets, 1.0 and −1.2 V for exfoliated $MoSe_2$ nanosheets and 1.0 and −1.3 V for exfoliated WSe_2 nanosheets. At these potentials, it is likely that there is chemical alteration of the surface structure of the TMD materials as a result of redox reactions of the material itself. This knowledge piqued our curiosity about the electrochemical behavior of the TMD materials after electrochemically oxidizing or reducing them at the chosen potentials. After the exfoliated MoS_2, WS_2, $MoSe_2$ and WSe_2 nanosheets were subject to chronoamperometric treatment at their respective potentials, we performed surface, structural and morphological characterization of the materials *via* X-ray photoelectron spectroscopy (XPS), Raman spectroscopy and high resolution transmission electron microscopy (HR-TEM) respectively, followed by cyclic voltammetric measurements to investigate the heterogeneous electron transfer (HET) rate of the oxidized, reduced and untreated TMD nanosheets. Using the Nicholson method,[30] the HET rates can be derived from correlating the peak-to-peak separation (ΔE_p) to the charge transfer rate (k^0_{obs}) where larger ΔE_p relates to slower HET rates. With the aid of two different redox probes: ferro/ferricyanide complex ($[Fe(CN)_6]^{4-/3-}$) and ruthenium(III/II)-hexamine complex ($[Ru(NH_3)_6]^{3+/2+}$), we are able to acquire electrochemical information about exfoliated MoS_2, WS_2, $MoSe_2$ and WSe_2 nanosheets as well as their oxidized and reduced forms.

Characterization of Electrochemically Treated TMDs. Structural and surface changes of TMDs may result from electrochemical treatment which in turn would be useful toward explaining the electrochemical and catalytic trends of the TMDs. XPS was performed to examine the surface elemental compositions and the high resolution XPS spectra are shown in Figure 2. Raman spectroscopy was conducted to evaluate structural information on the TMDs. Raman spectra is illustrated in Figure 3.

The MoS_2 nanosheets seem to preserve the semiconducting 2H phase after the exfoliation as evident in the XPS signals identified at 229 and 232 eV for Mo $3d_{5/2}$ and Mo $3d_{3/2}$ respectively. Subjecting the MoS_2 nanosheets to electrochemical oxidation or reduction treatment decreases its 2H-phase component. The oxidation of MoS_2 nanosheets is also confirmed by the increase in Mo^{6+} $3d_{5/2}$ and Mo^{6+} $3d_{3/2}$ signals at 233 and 236 eV to 28.1% while in the reduced MoS_2 nanosheets, the extent of oxidation is noted to be slightly lower. Dissimilar to MoS_2 nanosheets, $MoSe_2$ nanosheets contain a mixture of 2H- and 1T- phase. Redox treatment of $MoSe_2$ nanosheets elevated the contribution of the 1T-phase Mo $3d_{5/2}$ and Mo $3d_{3/2}$ signals to 17.0% in the oxidized and 12.2% in the reduced while the 2H-phase components declined to 40.9% in the oxidized and further depleted to 31.9% in the reduced. Mo^{6+} $3d_{5/2}$ and Mo^{6+} $3d_{3/2}$ signals of electrochemically treated $MoSe_2$ materials spiked to 42.1% when oxidized and a surprisingly higher intensity at 55.9% when reduced.

The WS_2 and WSe_2 nanosheets manifested 2H-phase W $4f_{7/2}$ and W $4f_{5/2}$ peaks at 32 and 34 eV. Reduction and oxidation of WS_2 nanosheets increased the amount of 1T-phase to 26.4% and 10.4% respectively. However, when WSe_2 nanosheets were subject to electrochemical oxidation or reduction, the 1T-phase was absent and this was accompanied by a higher proportion of 2H-phase at 55.1% in its oxidized state and 82.3% in its reduced state. W^{6+} $4f_{7/2}$ and W^{6+} $4f_{5/2}$ components of WS_2 occurring at binding energies of 36 and 38 eV were marginally reduced to 44.0% in oxidized WS_2 and dropped to 31.5% in reduced WS_2. Likewise, there was a minor drop to 44.9% in oxidized WSe_2 nanosheets and a substantial decline to 17.7% in reduced WSe_2 nanosheets.

Close inspection of the oxidized M(VI) component across the TMD materials, disregarding the type of

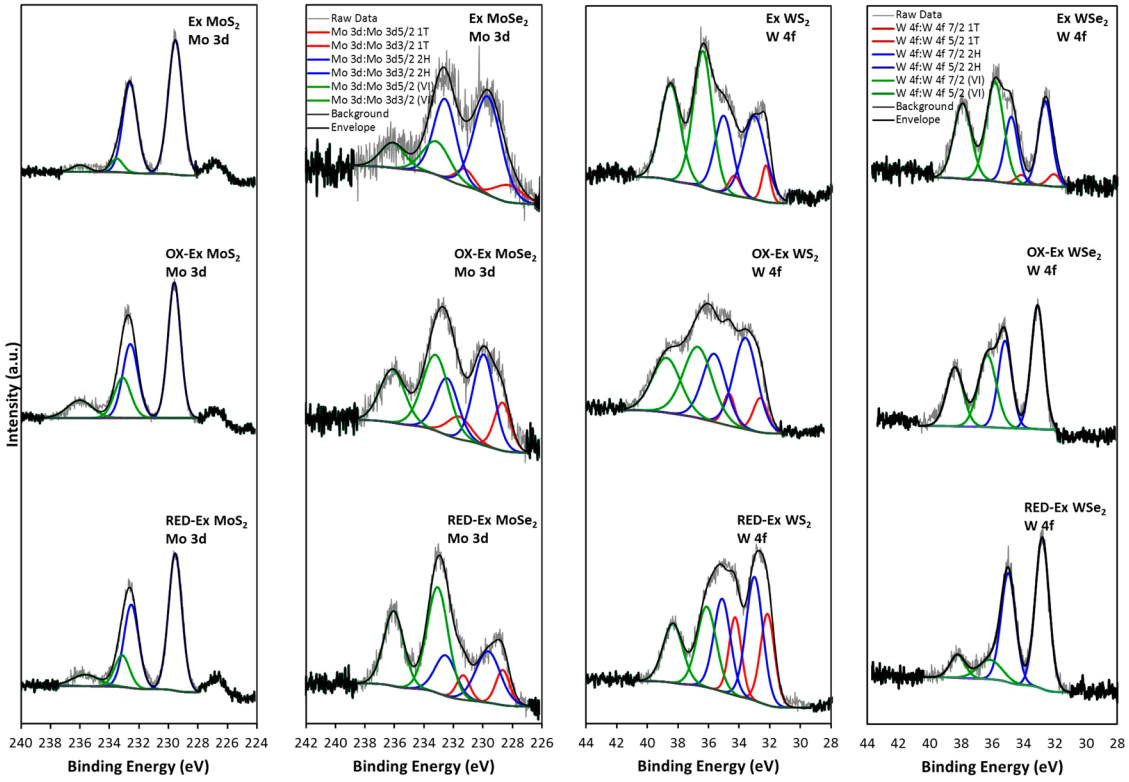

Figure 2. High resolution X-ray photoelectron spectra of the Mo 3d and W 4f regions of exfoliated MoS_2, $MoSe_2$, WS_2 and WSe_2 nanosheets before and after electrochemical treatment. Metallic 1T phase given in red, semiconducting 2H phase denoted in blue and oxidized (VI) state in green.

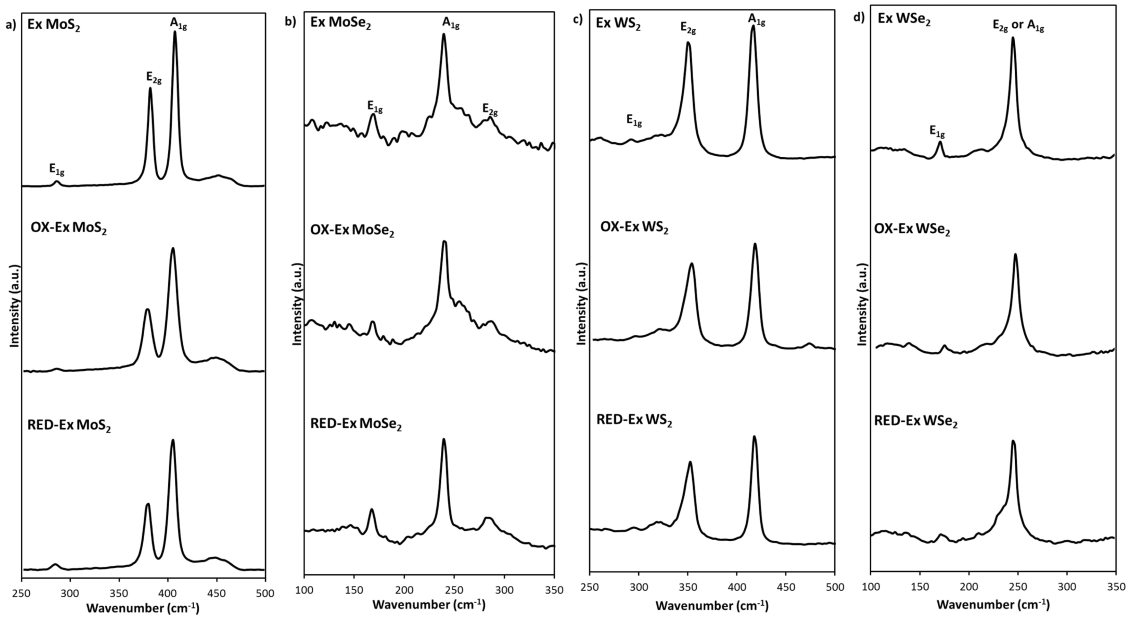

Figure 3. Raman spectra of exfoliated (a) MoS_2, (b) $MoSe_2$, (c) WS_2 and (d) WSe_2 nanosheets before and after electrochemical oxidation or reduction. λ_{exc} = 514.5 nm.

electrochemical treatment, reveals the trend of increasing M^{6+} contribution: MoS_2 (8.0%) < $MoSe_2$ (22.5%) < WS_2 (54.2%) < WSe_2 (57.2%). This finding coincides with earlier reports on WX_2 (where X= S or Se) are more readily oxidized than MoX_2[31] and MSe_2 (where M = Mo or W) more vulnerable to oxidation than MS_2.[32]

We next explore the effect of electrochemical treatment on the chalcogen-to-metal ratio (recorded in Table S1, SI) and deduced that electrochemical treatment varies the chalcogen-to-metal ratio in the Mo chalcogenides whereas the ratio remains relatively unaffected in W chalcogenides. Oxidizing MoS_2 produces

a higher chalcogen-to-metal ratio of 2.6 than when untreated. In turn, the high chalcogen-to-metal ratio depicts Mo metal deficiency largely due to the formation of MoO_4^{2-} and, to a smaller extent, the SO_4^{2-} species at oxidative potentials above 1.0 V *vs* Ag/AgCl.[33] Reducing MoS_2 results in a smaller chalcogen-to-metal ratio at 1.9 compared to the previous 2.2 in untreated. There is a dramatic difference in the chalcogen-to-metal ratio of $MoSe_2$ across its electrochemically treated and untreated states. At an anodic potential of above 1.0 V, $MoSe_2$ could generate elemental species in their highest oxidation states such as MoO_4^{2-} and SeO_4^{2-} at pH 7. In doing so, the chalcogen-to-metal ratio of $MoSe_2$ when oxidized is observed to decrease to 1.9 from 3.0 in untreated $MoSe_2$. Moreover, the further plunge in chalcogen-to-metal ratio of $MoSe_2$ to 1.1 upon reduction may be attributed to inherent reductions that produce HSe^- species[34] which deplete the Se chalcogen composition, inducing a Mo-enriched environment in reduced $MoSe_2$. In the situation of the W compounds, it appears that the chalcogen-to-metal ratio remains relatively stable across the oxidized, reduced and untreated states.

The Raman spectra in Figure 3 depict two predominant signals across all TMD materials: in-plane E_{2g} (shear) and the out-of-plane A_{1g} (breathing) modes. The in-plane E_{2g} mode has the metal and chalcogen atoms moving in opposite directions in-plane and can be distinguished from A_{1g} mode which has the metal atom stationary with chalcogen atoms moving out of the plane in opposite directions. The E_{1g} phonon is also discernible in all TMD materials. Because of its weak diagnostic trait, the E_{1g} mode is not of interest.

The A_{1g} phonon band of exfoliated MoS_2 nanosheets manifested a red shift of 2.0 cm^{-1} and broadened by 2.0 cm^{-1} when electrochemically reduced, whereas the E_{2g} band remains relatively unchanged. However, this trend is not replicated for other TMDs. Though it has been discovered that the E_{2g} mode is inert to electron doping, a red shift of the A_{1g} and its broadening are attributes of electron doping.[35,36] Such disparity of the phonon signals toward electron doping is explained by the stronger electron−phonon coupling of A_{1g} than E_{2g}. Hence, this observation in the MoS_2 nanosheets verifies that electrochemical reduction has effectively introduced electrons to into the MoS_2 system. Moreover, the decreased in frequency and line width broadening of the A_{1g} phonon after redox treatment corresponds to decreased number of layers.[37]

Raman shifts in exfoliated $MoSe_2$ nanosheets exhibit a trend contrary to MoS_2 upon electrochemical reduction. The A_{1g} phonon remains fixated at approximately 240 cm^{-1} with a gradual decrease in its full width at half-maximum (fwhm) from 10.5 to 9.5 in reduced $MoSe_2$. When electrochemically reduced, the E_{2g} mode observes a blue shift and slight broadening (0.8 cm^{-1}). Conversely, oxidized $MoSe_2$ undergoes a blue shift (1.4 cm^{-1}) in A_{1g} phonon and a sharp decline in fwhm (5.0 cm^{-1}) of the E_{2g} mode. There is also substantial changes to the $I(A_{1g})/I(E_{2g})$ ratio across $MoSe_2$ materials as a result of electrochemical treatment which is not noted in other TMDs.

While electrochemically treated WS_2 nanosheets reveal the stiffening of both E_{2g} and A_{1g} modes, we observe broadening in E_{2g} mode and decreased fwhm in A_{1g}. Reported for MoS_2, the line width of E_{2g} mode is less sensitive to changes in layer thickness but there is strong layer-dependence of the line width in A_{1g} phonon.[37] The reduced line width in A_{1g} mode after electrochemical treatment translates into presence of thicker layers,[38] often the bulk-like inner layers, which dominate the Raman intensity of the treated WS_2. More interestingly, WO_3 Raman signals[39] are also observed as illustrated in Figure S4 (SI). In untreated WS_2 nanosheets, we notice 2 narrow bands at 715 and 807 cm^{-1} that are typical features of WO_3. However, upon subjecting to oxidation or reduction, the 2 bands vanished and instead a broad signal at 645 cm^{-1} characteristic of hydrated WO_3 ($WO_3 \cdot xH_2O$) signal is observed. The presence of WO_3 moieties on the surface of WS_2 materials also coincides with significant percentage of W^{6+} components from our experimental XPS data and affirmed the presence of solid oxides in all WS_2 materials.

Exfoliated WSe_2 nanosheets are known to exhibit E_{2g} and A_{1g} phonons within close proximity of each other at 248 and 250 cm^{-1} to quote from literature.[40] Our experimental Raman band of WSe_2 materials occurring at about 247 cm^{-1} concurs with literature values.

In addition, the morphological changes of the treated TMDs (MoS_2, $MoSe_2$, WS_2, WSe_2) were investigated by high-resolution transmission electron microscopy (HR-TEM), see Figure S5 (SI). After the anodic and cathodic treatment we could notice the presence of a more extensive amorphous (noncrystalline) phase together with the crystalline one in MoS_2 which was prominent in the untreated material. No other significant differences could be highlighted between the materials upon the electrochemical treatment. It is crucial to note that HR-TEM probes only a very small portion of the sample and therefore does not provide overall information on the sample properties. Electrochemical behavior is strongly influenced by the overall chemical and physical properties of the material surface, which can be obtained by means of spectroscopic techniques such as XPS and Raman, as discussed above.

Heterogeneous Electron Transfer (HET) at Activated TMDs Based on $[Fe(CN)_6]^{4-/3-}$ Redox Probe. Extensive research on $[Fe(CN)_6]^{4-/3-}$ redox probe in the past has determined its surface sensitivity[41] toward various electrode materials. The surface sensitive nature will be advantageous when evaluating HET rates of

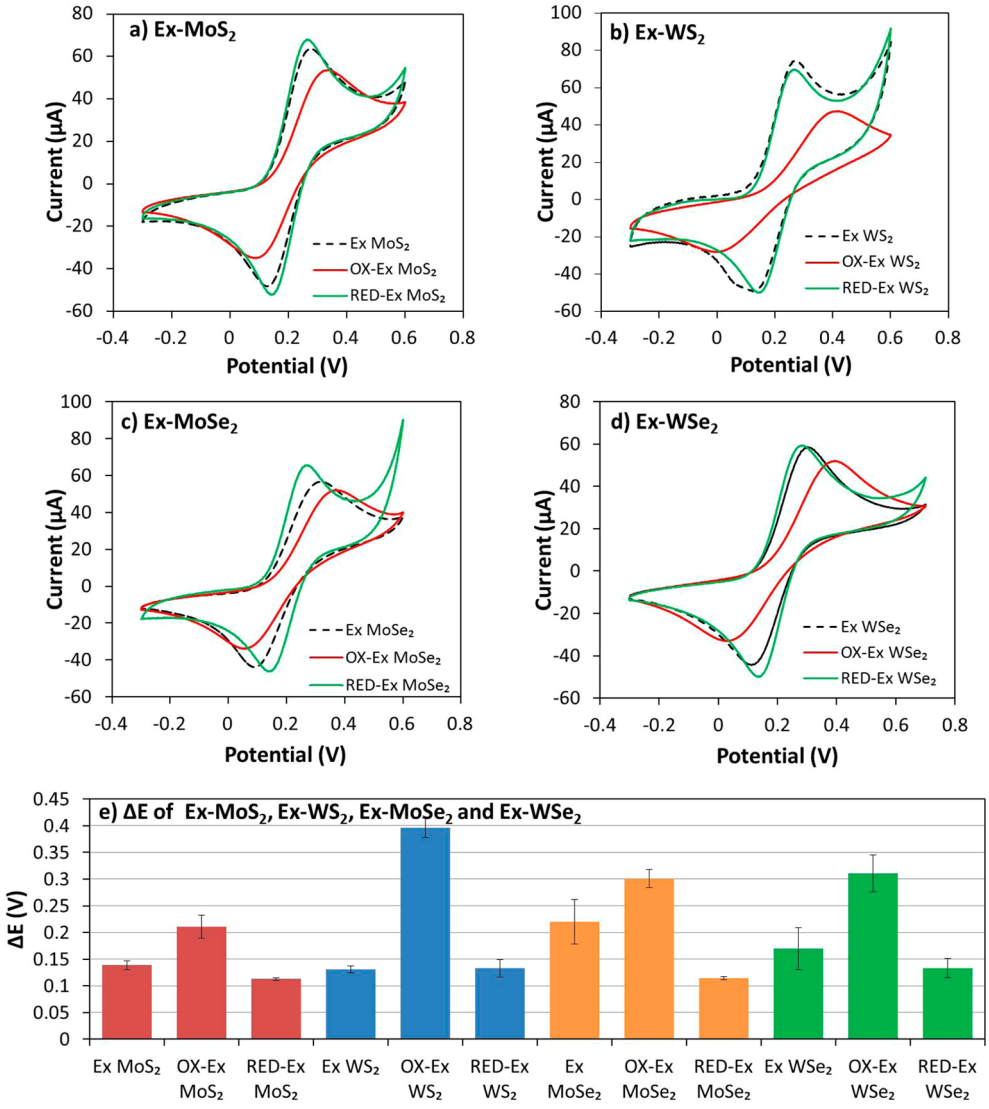

Figure 4. Cyclic voltammograms of 5 mM $[Fe(CN)_6]^{4-/3-}$ on exfoliated (a) MoS_2 nanosheets, (b) WS_2 nanosheets, (c) $MoSe_2$ nanosheets and (d) WSe_2 nanosheets before and after electrochemical treatment. (e) Summary of peak-to-peak separations of treated and untreated TMD materials with their corresponding error bars. Conditions: background electrolyte, KCl (0.1 M); scan rate, 100 mV s^{-1}; all measurements are performed relative to the Ag/AgCl reference electrode.

the exfoliated MoS_2, WS_2, $MoSe_2$ and WSe_2 nanosheets in the presence of $[Fe(CN)_6]^{4-/3-}$. Figure 4 records the voltammetric profiles of $[Fe(CN)_6]^{4-/3-}$ in 0.1 M KCl on the exfoliated TMD nanosheets and their oxidized or reduced forms resulting from electrochemical treatment.

As reflected in Figure 4a (and Table S3, SI), the untreated MoS_2 nanosheets had a ΔE_p of 0.139 V and a k^0_{obs} calculated to be 2.5×10^{-3} cm s^{-1}. When subject to electrochemical treatment, oxidized MoS_2 nanosheets had ΔE_p of 0.21 V ($k^0_{obs} = 9.5 \times 10^{-4}$ cm s^{-1}) and reduced MoS_2 nanosheets yielded ΔE_p of 0.11 V ($k^0_{obs} = 3.6 \times 10^{-3}$ cm s^{-1}). In Figure 4c, $MoSe_2$ nanosheets displayed ΔE_p of 0.22 V ($k^0_{obs} = 8.4 \times 10^{-4}$ cm s^{-1}) when not treated, ΔE_p of 0.30 V ($k^0_{obs} = 2.8 \times 10^{-4}$ cm s^{-1}) when oxidized and ΔE_p of 0.11 V ($k^0_{obs} = 3.5 \times 10^{-3}$ cm s^{-1}) when reduced. On the basis of these HET rates, we note that both exfoliated MoS_2 and $MoSe_2$ nanosheets exhibited faster HET rates in their reduced states than when untreated while their oxidized states had slower HET rates. As MoS_2 and $MoSe_2$ compounds[42] are usually n-type TMDs, such phenomenon may be supported by the semiconductor band theory.[43] Oxidative treatments of the MoS_2 and $MoSe_2$ nanosheets at positive potentials at 1.1 and 1.0 V respectively, which exist above their flatband potential, conduct electrons away from the interface and a depletion region ensues. Deficiency of electrons at the interface hampers electron transfer between the electrolyte and the electrode surface modified with oxidized MoS_2 or $MoSe_2$. This is evident in the large ΔE_p and low HET rates of the oxidized Mo compounds. In a similar manner, when the MoS_2 and $MoSe_2$ nanosheets are electrochemically reduced at respective negative potentials of −1.3 and −1.2 V, electrons gather at the interface which creates an accumulation region.

In doing so, the electron rich region at the interface provides a steady stream of electrons for charge transfer and accelerates HET rates of the reduced Mo compounds. WSe_2 nanosheets also comply with same trend as the Mo compounds wherein a higher HET rate of 2.7×10^{-3} cm s^{-1} was demonstrated in reduced WSe_2 and a slower rate at 2.5×10^{-4} cm s^{-1} for oxidized WSe_2 nanosheets. Consistent with MoS_2, $MoSe_2$ and WSe_2 nanosheets, the HET rate of WS_2 nanosheets was slowed down upon oxidation. However, there was negligible improvement of the HET rate of reduced WS_2 nanosheets from the untreated WS_2 nanosheets unlike enhanced HET performance of reduced MoS_2, $MoSe_2$ and WSe_2 nanosheets compared to their untreated counterparts. The HET rates of reduced and untreated WS_2 nanosheets are comparable to each other, the reduced at 2.7×10^{-3} cm s^{-1} and the untreated at 2.8×10^{-3} cm s^{-1}. Perhaps, apart from explanation using the semiconductor band theory, there are other factors inherent to the TMD material that comes into play.

Upon closer scrutiny of Figure 4e, we discover that the type of metal and chalcogen are also imperative to the HET rates in TMD materials. Considering the effect of the metal component, we juxtapose treated and untreated MoS_2 with WS_2 nanosheets and $MoSe_2$ with WSe_2 nanosheets keeping the chalcogen component constant. It is interesting to note that Mo compounds are more effectively activated by electrochemical reduction than W compounds in the aspect of electron transfer rates. Reduced MoS_2 afforded a HET rate that is 1.4 times (42% increment) faster than its untreated state whereas HET rates of reduced and untreated WS_2 differed by an imperceptible 2%. Similarly, reduced $MoSe_2$ yielded a 4.2 times enhancement of HET rates relative to when untreated, while reduced WSe_2 was 1.6 times faster than untreated WSe_2. Complementing the findings on the activation of HET rates by reduction, oxidation of MoS_2 and WS_2 nanosheets impeded their electron transfer rates drastically. The deactivation of electrochemical property is more strongly felt in oxidized WS_2 than MoS_2. When oxidized, the HET rate of WS_2 plunged dramatically by 36.7 times its original rate, while oxidized MoS_2 had a HET rate 2.6 times slower than its untreated form. Therefore, reduced Mo compounds demonstrate markedly enhanced HET rates relative to W compounds and the deactivation of electrochemical property was more apparent in oxidized W compounds than Mo compounds. We proceed to investigate how the chalcogen type governs the electrochemical properties of the TMD materials with the metal kept unchanged. Comparisons between MoS_2 and $MoSe_2$ evince that reduced $MoSe_2$ portrayed a significantly improved HET rate compared to its untreated state than reduced MoS_2 with its untreated counterpart. Concurring with this trend, the reduced WSe_2 showed enhanced HET rate than when untreated, whereas HET rates of reduced WS_2 and its untreated state remained generally the same. From this, we deduce that there is a larger extent of electrochemical activation experienced in Se than S compounds. Among all the TMD materials, $MoSe_2$ consisting of Mo and Se components is most sensitive to electrochemical activation in the aspect of HET rates because there are crucial differences in the structures of its reduced, oxidized and untreated states. In turn, the active sites available for electron transfer in $MoSe_2$ materials vary most substantially than the rest of the TMD materials upon electrochemical treatment.

Heterogeneous Electron Transfer (HET) at Electrochemically Activated TMDs Based on $[Ru(NH_3)_6]^{2+/3+}$ Redox Probe. As an experimental control, the measurements were repeated in the presence of $[Ru(NH_3)_6]^{2+/3+}$ redox probe to ascertain the findings in $[Fe(CN)_6]^{4-/3-}$ probe. Unlike $[Fe(CN)_6]^{4-/3-}$, $[Ru(NH_3)_6]^{2+/3+}$ is known to be insensitive to surface functional groups.[44] After electrochemical oxidation or reduction, Figure 5 shows no compelling difference for all the TMD materials. Since the treated and untreated TMD materials exhibited different HET rates in $[Fe(CN)_6]^{4-/3}$, we have confirmed that oxidation or reduction treatments had chemically altered the surface composition of the materials.

Electrochemically Treated TMDs for Hydrogen Evolution Reaction (HER). Research into MoS_2 as hydrogen evolution electrocatalyst has garnered much success, prompting scientists to delve into other layered TMDs as sustainable electrocatalysts for hydrogen evolution reaction (HER). Encouraged by the discovery of enhanced heterogeneous electron transfer (HET) performance of Mo compounds and WSe_2 nanosheets after electrochemical reductive pretreatment, we opted to evaluate the effect of electrochemical pretreatments toward the catalytic HER performance of the TMDs. In particular, we want to determine if the catalytic properties of exfoliated MoS_2, WS_2, $MoSe_2$ and WSe_2 nanosheets can be altered by the application of a reductive or oxidative electrochemical treatment.

Figure 6 records the HER polarization curves of the transition metal dichalcogenide (TMD) materials before and after electrochemical treatment. Often exemplified as the best HER catalyst, Pt/C yields low Tafel slopes of 30 to 40 mV/dec[45] and is used as a yardstick in this experiment to gauge the efficiency of HER catalysis by the TMD materials. The experimental Tafel slope of 37.8 mV/dec for Pt/C is in good agreement with literature values. Polarization curve of bare GC is also included for reference because GC serves as the electrochemical transducer modified with the desired TMD.

Two commonly adopted HER performance indicators are the Tafel slope and the onset potential. The Tafel slope is the increase in overpotential required to elicit a magnitude rise in current density. Smaller Tafel

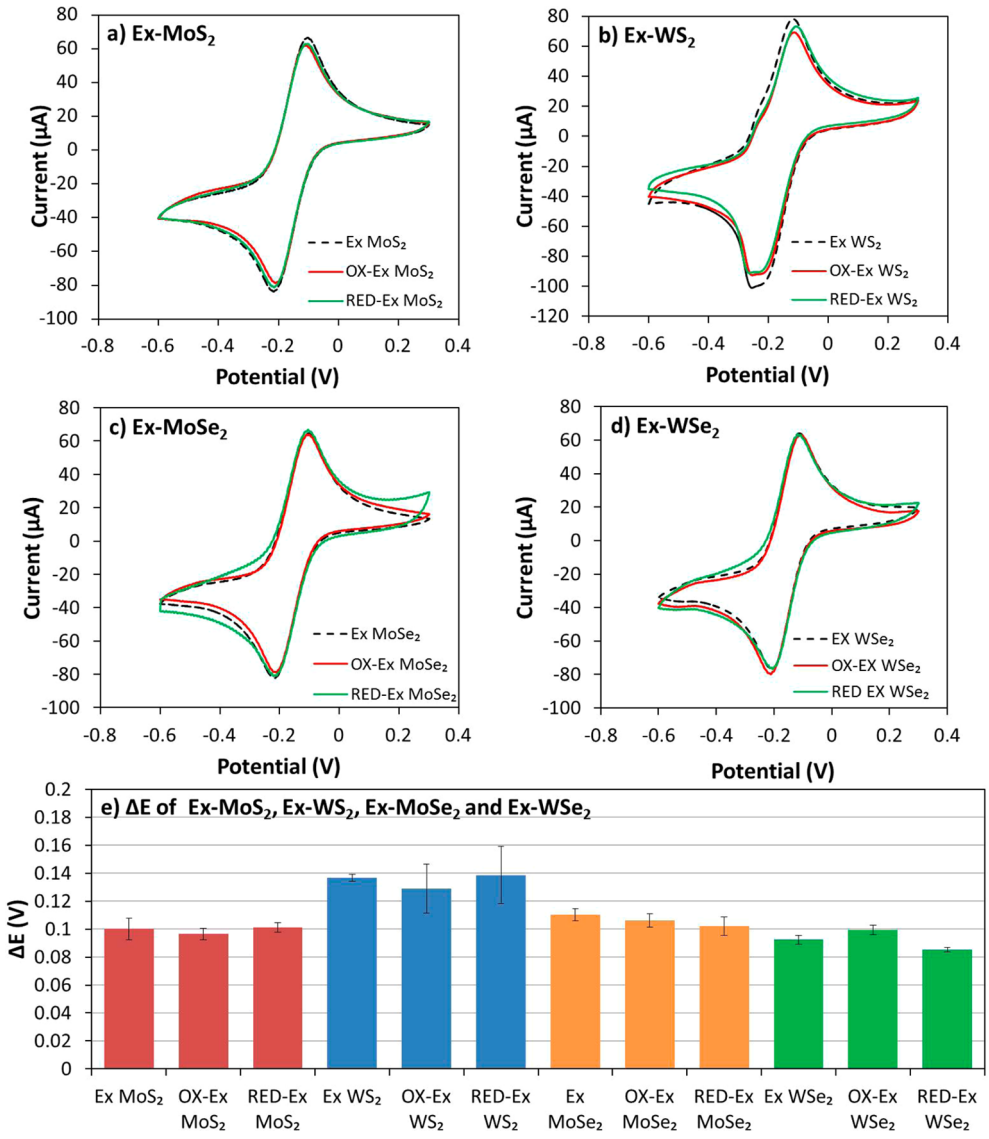

Figure 5. Cyclic voltammograms of 5 mM $[Ru(NH_3)_6]^{2+/3+}$ on exfoliated (a) MoS_2 nanosheets, (b) WS_2 nanosheets, (c) $MoSe_2$ nanosheets and (d) WSe_2 nanosheets before and after electrochemical treatment. (e) Summary of peak-to-peak separations of treated and untreated TMD materials with their corresponding error bars. Conditions: background electrolyte, KCl (0.1 M); scan rate, 100 mV s^{-1}; all measurements are performed relative to the Ag/AgCl reference electrode.

slopes are desirable for HER. Moreover, the Tafel slope elucidates the mechanism for HER on different TMD materials and its rate-determining step. In general, HER consists of two steps.[46,47] First is the Volmer adsorption step whereby the hydrogen binds to the catalyst (its binding site denoted as M*) as such: $H^+ + e + M^* \rightarrow M{-}H$ with a Tafel slope value of 120 mV/dec. Subsequently, it involves a desorption step either *via* the Heyrovsky process: $H^+ + e + M{-}H \rightarrow M^* + H_2$ at a Tafel slope value of 40 mV/dec, or the Tafel process: $2M{-}H \rightarrow 2M^* + H_2$ at a Tafel slope value of 30 mV/dec The onset potential is understood to be the potential at which the current density begins to fall steeply due to proton reduction. Across literature, the parameters in determining HER onset potentials fluctuate. We measure the onset potential as the potential corresponding to the current density of -0.1 mA cm^{-2}. The onset values for the TMD materials are provided in Figure S6 (SI) and will not be discussed in detail. Instead of onset potentials, we employ the overpotential at a current density of -10 mA cm^{-2} as a benchmark[48] because the pre-HER waves observed in WS_2, $MoSe_2$ and WSe_2 may thwart our evaluation of HER onset potentials.

At a current density of -10 mA cm^{-2}, the overpotentials for the TMD materials are summarized in Figure 6e as gathered from the polarization curves in Figure 6a and 6c. The HER catalytic trend across untreated TMD materials unveils $MoSe_2$ as the leading HER catalyst with the lowest overpotential at 0.37 V, followed by WS_2 with overpotential at 0.39 V and MoS_2 at 0.53 V and trailing behind is WSe_2 at highest overpotential at 0.76 V. Their Tafel slope values also reinforce this trend wherein $MoSe_2$ has the lowest Tafel slope at 86 mV/dec, followed by WS_2 and MoS_2 at

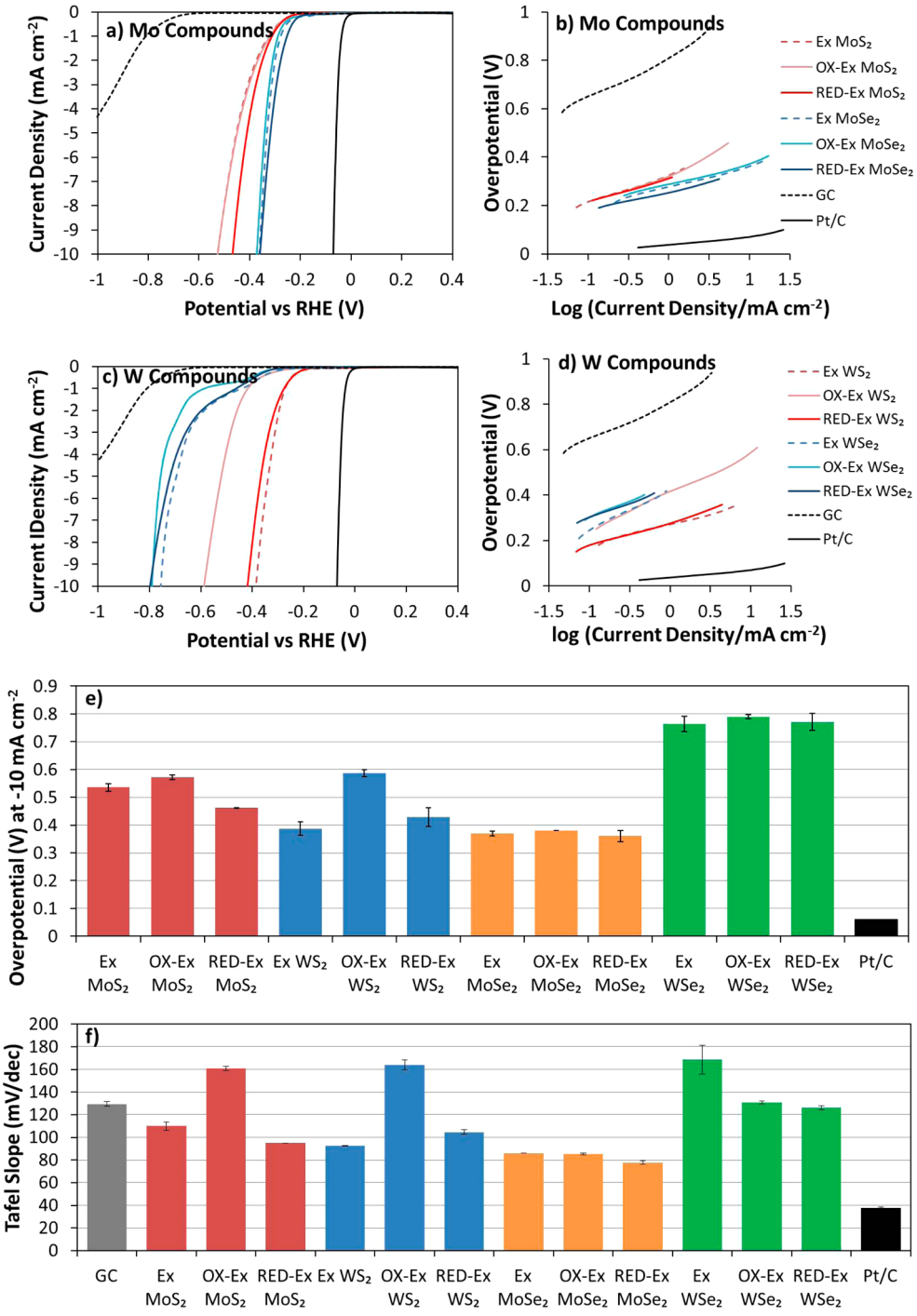

Figure 6. Linear sweep voltammograms for HER in acidic electrolyte on (a) MoS_2 and $MoSe_2$ nanosheets and their respective oxidized or reduced forms and (c) WS_2 and WSe_2 nanosheets and their respective oxidized or reduced forms. Tafel plots for (b) Mo compounds and (d) W compounds. Presented in bar charts are the averages of (e) overpotential at -10 mA cm^{-2} current density and (f) Tafel slopes with their corresponding error bars for all the materials. Conditions: background electrolyte, H_2SO_4 (0.5 M); scan rate, 2 mV s^{-1}; all measurements are performed relative to the Ag/AgCl reference electrode and corrected to reversible hydrogen electrode (RHE) potentials.

higher Tafel slopes of 93 and 110 mV/dec. The highest Tafel slope at 169 mV/dec is demonstrated in WSe_2. Furthermore, a density functional study led by Nørskov *et al.*[49] complements this HER catalytic trend. To quote from this study, $MoSe_2$ and WS_2 are armed with both their metal and chalcogen edges as active sites for HER. Conversely, MoS_2 and WSe_2 are less privileged, having either metal or chalcogen as active sites and not both. The primary active site for MoS_2 lies at the Mo-edge while WSe_2 utilizes Se-edge. The differential hydrogen free energies, ΔG_H, which are suitable markers of HER rate, of Mo- and Se- edge of $MoSe_2$ are found to be

more thermoneutral, with an optimal binding energy approximating zero,[50−52] than W- and S- edge of WS_2. ΔG_H of Mo-edge in MoS_2 and Se-edge in WSe_2 are comparable. Hence, the interplay of HER active sites and ΔG_H anticipate $MoSe_2$ to show the highest HER catalytic activity, followed closely by WS_2. Furthermore, 1T-phase obtained from XPS data may be adopted to account for the more efficient hydrogen evolution reaction occurring on the $MoSe_2$ catalyst than the MoS_2 catalyst. $MoSe_2$ comprises of a higher percentage of 1T-phase compared to MoS_2, which sees the absence of it. By the same token, WS_2 has a higher intensity of 1T-phase than WSe_2, which justifies the behavior of WS_2 as a better HER catalyst than WSe_2.

However, 1T-phase alone is inadequate to explain the extent of HER activation in the TMD materials because unlike 2H phase, which is thermodynamically stable in TMDs, the 1T phase existing in comparatively low amounts and less stable in atmosphere is prone to oxidation. Hence, chalcogen-to-metal ratio could also be a factor for consideration in such instances.

Out of all the TMD materials, electrochemical activation is found to be successful for MoS_2 material wherein the lowering of HER overpotential is apparent at a current density of -10 mA cm^{-2} when MoS_2 is electrochemically reduced. Unlike its untreated form, reduced MoS_2 depicts a smaller Tafel slope value at 95 mV/dec The catalytic site in MoS_2 is reported to be at the Mo-edge, specifically where the undercoordinated S exists.[53] Reduced MoS_2 is postulated to contain a marked increase in these HER catalytic zones and hence, displays an improved HER activity. The chalcogen-to-metal ratio derived from the XPS analysis gives credence to this hypothesis whereby reduced MoS_2 has a notably lower ratio than before treatment, indicative of the increase in Mo metal composition in MoS_2 after reduction and likely translates into more Mo-edge sites available for HER which activates the material for HER. Indeed, reduced MoS_2 behaving as a better HER electrocatalyst than when untreated concurs with our earlier electrochemical activation study[28] using MoS_2 nanosheets prepared from lithium intercalation with *n*-BuLi. In that study, the reduced MoS_2 nanosheets demonstrated enhanced HER catalysis than its untreated counterpart. At first sight, oxidized MoS_2 shows little deviation from its untreated counterpart as reflected in the almost overlapping HER polarization curves. Careful inspection discloses that there is slight increment in its HER overpotential to 0.57 V and a substantial rise in Tafel slope to 161 mV/dec pointing to an imperceptibly weaker HER activity in oxidized MoS_2 than its untreated form. A Tafel slope of 161 mV/dec transforms the HER rate-determining step in MoS_2 from a combination of Volmer-Heyrovsky processes to a Volmer process in its oxidized state. Previous research reports MoO_3 species formation when MoS_2 is electrochemically oxidized.[54] The hydrogen binding site occurring at the Mo-edge of MoS_2 is hindered as a result of MoO_3, which accounts for the imperceptibly lower catalytic behavior of oxidized MoS_2.

In stark contrast to effective activation of MoS_2 by electrochemical reduction for HER, WS_2 manifests electrochemical deactivation behavior when reduced and such deactivation occurs at a larger scale when oxidized. Most evident in oxidized WS_2, a high Tafel slope of 164 mV/dec with a corresponding large HER overpotential of 0.59 V is noted. Analogous to oxidized MoS_2, the slow step in HER has morphed from a joint Volmer−Heyrovsky process to the adsorption step in its oxidized state. Oxidation of WS_2 engenders WO_x compounds, predominantly existing as WO_3 due to the conversion of 4+ to 6+oxidation states in W. WO_x species modifies the W-edge, one of the HER binding site alongside S-edge, and deters hydrogen binding. In doing so, the W-edge sites available for binding are depleted, therefore impeding oxidized WS_2 as an electrocatalyst for HER. Another reason to justify the poor catalytic performance of oxidized WS_2 is based on XPS data. The 2H-phase of oxidized WS_2 stands at 45.6%, which is more than its untreated state, in turn, weaker HER efficiency is observed for oxidized WS_2. Moreover, the W^{6+} factor appears to be rather significant for oxidized WS_2 at 44.0%, which could influence the catalytic activity of the W-edge.

On the contrary to MoS_2 and WS_2, the HER catalytic activities of $MoSe_2$ and WSe_2 materials are less perturbed by electrochemical oxidation or reduction. The Tafel slopes and HER overpotential obtained for reduced, oxidized and untreated $MoSe_2$ differ marginally from each other by 7 mV/dec and 0.01 V. Tafel slopes of the $MoSe_2$ materials range from 78 to 86 mV/dec indicative of the rate-determining step for HER to be a concerted Volmer-Heyrovsky step regardless of electrochemical treatment. By the same token, WSe_2 materials exhibit relatively constant HER overpotentials of 0.78 to 0.76 V and Tafel slopes of beyond 120 mV/dec for its treated and untreated forms. Beyond 120 mV/dec, the slow step is predominantly the HER adsorption step for all WSe_2 materials. On the grounds of identical rate-determining steps for the reduced, oxidized and untreated states, the HER catalytic performance of $MoSe_2$ and WSe_2 materials are impervious to electrochemical activation. Despite the significant changes in chalcogen-to-metal ratio (Table S1, SI) in the oxidized, reduced and untreated $MoSe_2$, there is little effect of these differences on the HER efficiency of $MoSe_2$ materials as both metal and chalcogen edges are HER active.

Notably, there is a correlation between the chalcogen type and its susceptibility to electrochemical activation or deactivation for HER. Electrochemical treatment on TMD materials bearing the S chalcogen, in the case of MoS_2 and WS_2, influences their catalytic performance for HER. Conversely, TMD materials such

as $MoSe_2$ and WSe_2, which bear the Se chalcogen, are less affected by electrochemical treatment on their HER catalytic performance. Since Tafel slopes of the treated and untreated TMD materials lay beyond or fall within the range of Volmer and Heyrovsky processes, the hydrogen adsorption step contributes to their rate-determining step. The nature and location of the HER active sites in TMD materials govern its effect on electrochemical treatment for HER. Hydrogen binding site occurs at the Mo- and Se-edge for $MoSe_2$ whereas hydrogen binds solely at the Mo-edge in MoS_2. When subject to electrochemical reduction, Mo (VI) may be reduced to Mo (0) and this possibly improves the hydrogen binding function of the Mo-edge. This effect is more pronounced in MoS_2 because the active site at Mo-edge dominates the catalytic ability for HER. The HER catalytic ability of $MoSe_2$ comprises of both the Mo- and Se- edge and hence, less activated by electrochemical reduction than MoS_2. Considering WS_2 and WSe_2 materials, the active sites reside at the W- and S- edge for WS_2 and Se- edge in WSe_2. Electrochemical oxidation of WS_2 deactivates its catalytic performance for HER but HER ability of WSe_2 remains relatively unperturbed by oxidation. When electrochemically oxidized, W (IV) becomes W (VI) and WO_3 species[55] is reportedly formed. Therefore, hydrogen binding at the W-edge is restricted which impairs the HER catalytic ability of WS_2. Disparate from WS_2, W-edge is not the primary active site for HER in WSe_2 and hence WSe_2 is not deactivated by oxidation.

CONCLUSION

We explored the inherent electrochemistry of layered transition metal dichalcogenides (TMDs) materials, specifically MoS_2, WS_2, $MoSe_2$ and WSe_2 nanosheets. It has been determined that electrochemical reduction effectively activates the electrochemical property of MoS_2, $MoSe_2$ and WSe_2 nanosheets as substantiated by the improved heterogeneous electron transfer (HET) rates in their reduced forms. Among these three TMDs, the enhanced HET rate is most enhanced in reduced $MoSe_2$. Antithetical to electrochemical reduction, subjecting all the TMD materials to an electrochemical oxidation deteriorated their HET performance. Of which, the most drastic deactivation is experienced by the oxidized WS_2. The semiconductor band gap theory largely justifies the findings on variations in HET performance upon electrochemical treatment but other factors intrinsic to the TMDs may also contribute. There is also a correlation between the metal and chalcogen type on the extent of electrochemical activation. Considering metal component, Mo prevails over W, while in chalcogen type, Se exhibits higher sensitivity to electrochemical activation than S.

Successful electrochemical activation toward hydrogen evolution reaction (HER) is exclusively elucidated in MoS_2. The improved HER efficiency is evident in reduced MoS_2 demonstrating a lower Tafel slope and requiring a smaller HER overpotential at a current density of -10 mA cm^{-2} compared to its untreated counterpart. Conversely, the deactivation of catalytic performance is manifested in the electrochemical oxidation of WS_2 ensuing a higher Tafel slope and larger HER overpotential than when untreated. $MoSe_2$ and WSe_2 materials indicate that their HER performance is unreceptive to electrochemical oxidation or reduction. In general, electrochemical treatment exerts clout over TMDs containing the S chalcogen but yields no power over the compounds with the Se chalcogen. Differences in the characteristic number and type of active edge sites for HER in TMDs lead to their different HER behavior. Moreover, the oxidation or reduction processes that the TMDs are subject to may alter these edge sites, hence influencing the catalytic performance.

Therefore, we highlight here that TMDs have distinct responses to electrochemical treatment. In the aspect of HET, electrochemical treatment can be used to tweak the electrochemical properties of MoS_2, $MoSe_2$ and WSe_2 nanosheets whereby a reductive process elevates HET and an oxidative process deactivates the charge transfer performance. In the area of HER, electrochemical reduction is a success at activating MoS_2 and an oxidative treatment renders a weaker HER performance in WS_2 nanosheets. Knowledge of the TMD electrochemistry and the effect of electrochemical treatment on TMDs will be pivotal toward achieving desired aims in catalytic and electrochemical applications.

EXPERIMENTAL METHODS

Materials. Potassium ferrocyanide, hexaammineruthenium-(III) chloride, potassium chloride, potassium phosphate dibasic, sodium phosphate monobasic, sodium chloride, sulfuric acid and platinum on carbon were purchased from Sigma-Aldrich. Pt, Ag/AgCl and glassy carbon (GC) electrodes were purchased from CH Instruments, Texas, USA. Molybdenum disulfide, molybdenum diselenide, tungsten disulfide, tungsten diselenide (<2 μm), sodium and *tert*-butyllithium (1.7 M in pentane) were obtained from Sigma-Aldrich, Czech Republic. Hexane was obtained from Lach-ner, Czech Republic. Argon (99.9999% purity) was obtained from SIAD, Czech Republic.

Apparatus. X-ray photoelectron spectroscopy (XPS) was performed with a Phoibos 100 spectrometer with a monochromatic Mg K_α X-ray source (SPECS, Germany). Survey and high-resolution spectra were obtained for Mo 3d, W 4f, S 2p and Se 3d. The relative sensitivity factors were also adopted for the calculation of chalcogen-to-metal ratios and for deconvolution of oxidized states, 2H and 1T phases in the Mo and W compounds.

Raman spectroscopy was executed on a confocal micro-Raman LabRam HR instrument (Horiba Scientific) in backscattering geometry with a CCD detector, using an argon ion laser at an excitation wavelength of 514.5 nm and a 100× objective

mounted on an Olympus optical microscope. The laser spot has a diameter of about 5 μm across. The initial calibration was performed with a silicon reference at 520 cm^{-1}.

High resolution transmission electron microscopy (HR-TEM) was performed using Jeol 2100 TEM (Jeol, Japan) operating at 200 kV.

Voltammetric measurements were recorded on a μAutolab III electrochemical analyzer (Eco Chemie B.V., Utrecht, The Netherlands) with the software NOVA version 1.8 (Eco Chemie). Electrochemical measurements of the transition metal dichalcogenide (TMD) materials were performed in a 5 mL voltammetric cell at room temperature (25 °C) in a three electrode configuration. A platinum electrode and an Ag/AgCl electrode functioned as auxiliary and reference electrodes, respectively and a glassy carbon (GC, 3 mm diameter) electrode was adopted as the working electrode.

Procedures. *Exfoliation Procedure of Transition Metal Dichalcogenide (TMD).* The TMDs were exfoliated using the chemical intercalation method. The intercalation procedure was performed in the glovebox with Ar atmosphere (O_2 and H_2O below 0.1 ppm). Each of the bulk TMD (in powder form, Sigma-Aldrich) was dried at 100 °C for 48 h before insertion into glovebox which was kept at a constant temperature of 20 °C using a temperature conditioning system during the entire intercalation process. Li-intercalation process was carried out by stirring 3 g of the bulk TMD powder in 20 mL of 1.7 M *tert*-butyllithium in pentane for 72 h at 20 °C under argon atmosphere. To avoid contamination due to fluorine, a glass-coated magnetic stir bar was used instead of the standard PTFE-coated magnetic stir bar. The flask containing the reaction mixture was capped with a rubber septum with an inserted needle head to prevent the buildup of pressure in the reaction flask and minimize evaporative loss of volatile pentane solvent. Li-intercalated TMD was separated from excess intercalant by suction filtration *via* a 0.45 μm nylon membrane. Filtered material was washed three times with 30 mL of hexane (dried over sodium). The exfoliated material was dispersed in 100 mL of water and ultrasonicated for 15 min. Purification and separation were performed by repeated centrifugation (18000*g*) and redispersion in water until the conductivity was below 20 μS. Finally, the obtained TMD nanosheets were dried in a vacuum oven at 50 °C for 48 h prior to further use.

Inherent Electrochemistry and Activation Studies on Exfoliated Transition Metal Dichacolgenide (TMD) Nanosheets. Fundamental electrochemical studies were performed in 50 mM phosphate buffered saline (PBS) as the background electrolyte at pH 7. All cyclic voltammetry experiments were conducted at a scan rate of 100 mV s^{-1}. The voltammetric scan began at 0 V; the potential at which redox processes were not expected to occur,[56] and scanned toward 1.8 V followed by a reverse sweep to −1.8 V for the anodic study and first toward −1.8 V followed by a reverse sweep to 1.8 V for the cathodic study before returning to 0 V. The exfoliated MoS_2, $MoSe_2$, WS_2 and WSe_2 nanosheets were prepared in concentrations of 1 mg mL^{-1} in ultrapure water and subject to first-time ultrasonication for 1.5 h to attain homogeneous dispersions. Prior to each electrochemical measurement, the samples were ultrasonicated for a period of 10 min to maintain the well-dispersed suspension of the desired material. 4.0 μL aliquot of the suspension was then drop casted on a GC electrode and dried to yield an electrode surface modified with 4.0 μg film of the desired material.

Electrochemical activation was performed by applying an oxidation or reduction potential for a period of 300 s to procure their oxidized or reduced forms. For different TMD samples, the treatment was done in PBS pH 7 at a unique potential determined by the redox peaks in the study of their inherent electrochemistry. Exfoliated MoS_2 nanosheets were treated at +1.1 V (oxidation) or −1.3 V (reduction), exfoliated $MoSe_2$ nanosheets were treated at +1.0 V (oxidation) or −1.2 V (reduction), exfoliated WS_2 nanosheets were treated at +1.2 V (oxidation) or −1.6 V (reduction), and exfoliated WSe_2 nanosheets were treated at +1.0 V (oxidation) or −1.3 V (reduction). After treatment, the electrode was dipped in distilled water to rinse off any adsorbed materials and tested for heterogeneous electron transfer (HET) rate using cyclic voltammetry at a scan rate of 100 mV s^{-1} in the presence of potassium ferrocyanide (5 mM) or hexaammineruthenium(III) chloride (5 mM) redox probes in potassium chloride (0.1 M) as the supporting electrolyte.

The k^0_{obs} values were calculated using the method devised by Nicholson[30] that relates ΔE_p to a dimensionless parameter Ψ and consequently into $k^0_{obs.}$ The roughness of the electrode was not considered in the calculation of $k^0_{obs.}$ The diffusion coefficient $D = 7.26 \times 10^{-6}$ cm^2 s^{-1} was used to compute k^0_{obs} values for $[Fe(CN)_6]^{4-/3-}$.[57]

Hydrogen Evolution Reaction (HER) Studies on Exfoliated Transition Metal Dichacolgenide (TMD) Nanosheets. The hydrogen evolution reaction (HER) efficiency of TMD materials were tested on glassy carbon (GC) electrodes. The GC electrode surface was renewed before modification with TMD materials using a 0.05 μm alumina particle slurry on a polishing pad and washing with ultrapure water. The desired materials encompassing exfoliated MoS_2, $MoSe_2$, WS_2 and WSe_2 nanosheets and Pt/C were prepared in suspensions of 1 mg mL^{-1} in ultrapure water. These suspensions were ultrasonicated for 10 min to achieve homogeneity. The materials were immobilized on the GC electrode by depositing 4.0 μL aliquot of the suspended materials on the electrode surface. The solvent was left to evaporate at room temperature to yield a randomly distributed film of 4.0 μg of desired materials on the GC electrode surface.

Similar to the HET measurements, activation of the exfoliated MoS_2, $MoSe_2$, WS_2 and WSe_2 nanosheets was performed at pH 7.0 by applying their respective redox potentials for 300 s. HER measurements of these TMD materials were carried out using linear sweep voltammetry at a scan rate of 2 mV s^{-1} in 0.5 M H_2SO_4 electrolyte.

Linear sweep voltammograms are presented *versus* the reversible hydrogen electrode (RHE) using and the measured potentials are calculated using this equation[58] $E_{RHE} = E_{Ag/AgCl} + 0.059 \times pH + E^0_{Ag/AgCl}$ where $E_{Ag/AgCl}$ is the measured potential, pH of 0.5 M H_2SO_4 electrolyte is zero, and $E^0_{Ag/AgCl}$ refers to the standard potential of Ag/AgCl (1 M KCl) at 25 °C, which is 0.235 V.

Conflict of Interest: The authors declare no competing financial interest.

Acknowledgment. M.P. acknowledges funding from Ministry of Education (Singapore) from Tier 1 RGT1/13. Z.S. and J.L. were supported by Czech Science Foundation (GACR No. 15-07912S) and by Specific University Research (MSMT No. 20/2015).

Supporting Information Available: Cyclic voltammograms illustrating inherent electrochemistry of the oxides of molybdenum and tungsten; wide-scan and high resolution X-ray photoelectron spectra; tabulated elemental atomic compositions based on XPS; tabulated peak data from Raman spectroscopy; wide-range range Raman spectra; high-resolution TEM images; tabulated HET constants of TMDs; onset HER potentials of the TMDs. This material is available free of charge *via* the Internet at http://pubs.acs.org.

REFERENCES AND NOTES

1. Novoselov, K. S.; Geim, S. V.; Morozov, S. V.; Jiang, D.; Zhang, Y.; Dubonos, S. V.; Grigorieva, I. V.; Firsov, A. A. Electric Field Effect in Atomically Thin Carbon Films. *Science* **2004**, *306*, 666–669.
2. Huang, X.; Yin, Z.; Wu, S.; Qi, X.; He, Q.; Zhang, Q.; Yan, Q.; Boey, F.; Zhang, H. Graphene-Based Materials: Synthesis, Characterization, Properties, and Applications. *Small* **2011**, *7*, 1876–1902.
3. Claus, F. L. *Solid Lubricants and Self-Lubricating Solids*; Academic Press: New York, 1972.
4. Splendiani, A.; Sun, L.; Zhang, Y.; Li, T.; Kim, J.; Chim, C.-Y.; Galli, G.; Wang, F. Emerging Photoluminescence in Monolayer MoS_2. *Nano Lett.* **2010**, *10*, 1271–1275.
5. Xiao, D.; Liu, G.-B.; Feng, W.; Xu, X.; Yao, W. Coupled Spin and Valley Physics in Monolayers of MoS_2 and Other Group-VI Dichalcogenides. *Phys. Rev. Lett.* **2012**, *108*, 196802−1–196802−5.
6. Neville, R. A.; Evans, B. L. The Band Edge Excitons in 2H-MoS_2. *Phys. Status Solidi B* **1976**, *73*, 597–606.

7. Roxlo, C. B.; Chianelli, R. R.; Deckman, H. W.; Ruppert, A. F.; Wong, P. P. Bulk and Surface Optical Absorption in Molybdenum Disulfide. *J. Vac. Sci. Technol., A* **1987**, *5*, 555–557.
8. Li, T. S.; Galli, G. L. Electronic Properties of MoS_2 Nanoparticles. *J. Phys. Chem. C* **2007**, *111*, 16192–16196.
9. Eda, G.; Yamaguchi, H.; Voiry, D.; Fujita, T.; Chen, M.; Chhowalla, M. Photoluminescence from Chemically Exfoliated MoS_2. *Nano Lett.* **2011**, *11*, 5111–5116.
10. Fang, H.; Chuang, S.; Chang, T. C.; Takei, K.; Takahashi, T.; Javey, A. High-Performance Single Layered WSe_2 p-FETs with Chemically Doped Contacts. *Nano Lett.* **2012**, *12*, 3788–3792.
11. Li, Y.; Wang, H.; Xie, L.; Liang, Y.; Hong, G.; Dai, H. MoS_2 Nanoparticles Grown on Graphene: An Advanced Catalyst for the Hydrogen Evolution Reaction. *J. Am. Chem. Soc.* **2011**, *133*, 7296–7299.
12. Merki, D.; Fierro, S.; Vrubel, H.; Hu, X. Amorphous Molybdenum Sulfide Films as Catalysts for Electrochemical Hydrogen Production in Water. *Chem. Sci.* **2011**, *2*, 1262–1267.
13. Cortright, R. D.; Davda, R. R.; Dumesic, J. A. Hydrogen from Catalytic Reforming of Biomass-Derived Hydrocarbons in Liquid Water. *Nature* **2002**, *418*, 964–967.
14. Kye, J.; Shin, M.; Lim, B.; Jang, J.-W.; Oh, I.; Hwang, S. Platinum Monolayer Electrocatalyst on Gold Nanostructures on Silicon for Photoelectrochemical Hydrogen Evolution. *ACS Nano* **2013**, *7*, 6017–6023.
15. Sun, L.; Ca, D.; Cox, J. Electrocatalysis of the Hydrogen Evolution Reaction by Nanocomposites of Poly(amidoamine)-Encapsulated Platinum Nanoparticles and Phosphotungstic Acid. *J. Solid State Electrochem.* **2005**, *9*, 816–822.
16. Pumera, M.; Sofer, Z.; Ambrosi, A. Layered Transition Metal Dichalcogenides for Electrochemical Energy Generation and Storage. *J. Mater. Chem. A* **2014**, *2*, 8981–8987.
17. Chhowalla, M.; Shin, H. S.; Eda, G.; Li, L.-J.; Loh, K. P.; Zhang, H. The Chemistry of Two-Dimensional Layered Transition Metal Dichalcogenide Nanosheets. *Nat. Chem.* **2013**, *5*, 263–275.
18. Kibsgaard, J.; Chen, Z.; Reinecke, B. N.; Jaramillo, T. F. Engineering the Surface Structure of MoS_2 to Preferentially Expose Active Edge Sites for Electrocatalysis. *Nat. Mater.* **2012**, *11*, 963–969.
19. Choi, W. I.; Wood, B. C.; Schwegler, E.; Ogitsu, T. Site-Dependent Free Energy Barrier for Proton Reduction on MoS_2 Edges. *J. Phys. Chem. C* **2013**, *117*, 21772–21777.
20. Kong, D.; Wang, H.; Cha, J. J.; Pasta, M.; Koski, K. J.; Yao, J.; Cui, Y. Synthesis of MoS_2 and $MoSe_2$ Films with Vertically Aligned Layers. *Nano Lett.* **2013**, *13*, 1341–1347.
21. Wang, H.; Kong, D.; Johanes, P.; Cha, J. J.; Zheng, G.; Yan, K.; Liu, N.; Cui, Y. $MoSe_2$ and WSe_2 Nanofilms with Vertically Aligned Molecular Layers on Curved and Rough Surfaces. *Nano Lett.* **2013**, *13*, 3426–3433.
22. Firmiano, E.G. S.; Cordeiro, M. A. L.; Rabelo, A. C.; Dalmaschio, C. J.; Pinheiro, A. N.; Pereira, E. C.; Leite, E. R. Graphene Oxide as a Highly Selective Substrate to Synthesize a Layered MoS_2 Hybrid Electrocatalyst. *Chem. Commun.* **2012**, *48*, 7687–7689.
23. Zhou, T.; Yin, H.; Liu, Y.; Chai, Y.; Zhang, J.; Liu, C. Synthesis, Characterization and HDS Activity of Carbon-Containing Ni−Mo Sulfide Nano-Spheres. *Catal. Lett.* **2010**, *134*, 343–350.
24. Liu, B.; Chai, Y.; Liu, Y.; Wang, Y.; Liu, Y.; Liu, C. A Simple Method for Preparation of Presulfided Eggshell CoMoS/γ-Al_2O_3 Catalysts for Hydrodesulfurization of Dibenzothiophene. *Fuel* **2012**, *95*, 457–463.
25. Okamoto, Y.; Hioka, K.; Arakawa, K.; Fujikawa, T.; Ebihara, T.; Kubota, T. Effect of Sulfidation Atmosphere on the Hydrodesulfurization Activity of SiO_2-Supported Co−Mo Sulfide Catalysts: Local Structure and Intrinsic Activity of the Active Sites. *J. Catal.* **2009**, *268*, 49–59.
26. Merki, D.; Vrubel, H.; Rovelli, L.; Fierro, S.; Hu, X. Fe, Co, and Ni Ions Promote the Catalytic Activity of Amorphous Molybdenum Sulfide Films for Hydrogen Evolution. *Chem. Sci.* **2012**, *3*, 2515–2525.
27. Álvarez, L.; Berhault, G.; Alonso-Nuñez, G. Unsupported NiMo Sulfide Catalysts Obtained from Nickel/Ammonium and Nickel/Tetraalkylammonium Thiomolybdates: Synthesis and Application in the Hydrodesulfurization of Dibenzothiophene. *Catal. Lett.* **2008**, *125*, 35–45.
28. Chia, X.; Ambrosi, A.; Sedmidubský, D.; Sofer, Z.; Pumera, M. Precise Tuning of the Charge Transfer Kinetics and Catalytic Properties of MoS_2 Materials *via* Electrochemical Methods. *Chem.—Eur. J.* **2014**, *20*, 17426–17432.
29. Eng, A.Y.S.; Ambrosi, A.; Sofer, Z.; Šimek, P.; Pumera, M. Electrochemistry of Transition Metal Dichalcogenides: Strong Dependence on the Metal-to-Chalcogen Composition and Exfoliation Method. *ACS Nano* **2014**, *8*, 12185–12198.
30. Nicholson, R. S. Theory and Application of Cyclic Voltammetry for Measurement of Electrode Reaction Kinetics. *Anal. Chem.* **1965**, *37*, 1351–1355.
31. Miremadi, B. K.; Morrison, S. R. The Intercalation and Exfoliation of Tungsten Disulfide. *J. Appl. Phys.* **1988**, *63*, 4970–4974.
32. Jaegermaan, W.; Schmeisser, D. Reactivity of Layer Type Transition Metal Chalcogenides Towards Oxidation. *Surf. Sci.* **1986**, *165*, 143–160.
33. Bouroushian, M. *Electrochemistry of Metal Chalcogenides*; Springer-Verlag: Berlin, 2010.
34. Saji, V. S.; Lee, C.-W. Selenium Electrochemistry. *RSC Adv.* **2013**, *3*, 10058–10077.
35. Tongay, S.; Zhou, J.; Ataca, C.; Lo, K.; Matthews, T. S.; Li, J.; Grossman, J. C.; Wu, J. Thermally Driven Crossover from Indirect toward Direct Bandgap in 2D Semiconductors: $MoSe_2$ *versus* MoS_2. *Nano Lett.* **2012**, *12*, 5576–5580.
36. Chakraborty, B.; Bera, A.; Muthu, D. V. D.; Bhowmick, S.; Waghmare, U. V.; Sood, A. K. Symmetry-Dependent Phonon Renormalization in Monolayer MoS_2 Transistor. *Phys. Rev. B: Condens. Matter Mater. Phys.* **2012**, *85*, 161403.
37. Lee, C.; Yan, H.; Brus, L. E.; Heinz, T. F.; Hone, J.; Ryu, S. Anomalous Lattice Vibrations of Single- and Few-Layer MoS_2. *ACS Nano* **2010**, *4*, 2695–2700.
38. Ramakrishna Matte, H. S. S.; Gomathi, A.; Manna, A. K.; Late, D. J.; Datta, R.; Pati, S. K.; Rao, C. N. R. MoS_2 and WS_2 Analogues of Graphene. *Angew. Chem., Int. Ed.* **2010**, *49*, 4059–4062.
39. Daniel, M. F.; Desbat, B.; Lasseques, J. C. Infrared and Raman Study of WO_3 Tungsten Trioxides and WO_3, xH_2O Tungsten Trioxide Tydrates. *J. Solid State Chem.* **1987**, *67*, 235–247.
40. Tonndorf, P.; Schmidt, R.; Böttger, P.; Zhang, X.; Börner, J.; Liebig, A.; Albrecht, M.; Kloc, C.; Gordan, O.; Zahn, D. R. T.; de Vasconcellos, S. M.; Bratschitsch, R. Photoluminescence Emission and Raman Response of Monolayer MoS_2, $MoSe_2$, and WSe_2. *Opt. Express* **2013**, *21*, 4908–4916.
41. McCreery, R. L. Advanced Carbon Electrode Materials for Molecular Electrochemistry. *Chem. Rev.* **2008**, *108*, 2647–2687.
42. Tongay, S.; Zhou, J.; Ataca, C.; Liu, J.; Kang, J. S.; Matthews, T. S.; You, L.; Li, J.; Grossman, J. C.; Wu, J. Broad-Range Modulation of Light Emission in Two-Dimensional Semiconductors by Molecular Physisorption Gating. *Nano Lett.* **2013**, *13*, 2831–2836.
43. Bott, A. W. Electrochemistry of Semiconductors. *Curr. Sep.* **1998**, *17*, 87–91.
44. Chen, P. H.; McCreery, R. L. Control of Electron Transfer Kinetics at Glassy Carbon Electrodes by Specific Surface Modification. *Anal. Chem.* **1996**, *68*, 3958–3965.
45. Conway, B. E.; Tilak, B. V. Interfacial Processes Involving Electrocatalytic Evolution and Oxidation of H_2, and the Role of Chemisorbed H. *Electrochem. Acta* **2002**, *47*, 3571–3594.
46. Bockris, J. O. M.; Potter, E. C. The Mechanism of the Cathodic Hydrogen Evolution Reaction. *J. Electrochem. Soc.* **1952**, *99*, 169–186.
47. Thomas, J. G. Kinetics of Electrolytic Hydrogen Evolution and the Adsorption of Hydrogen by Metals. Trans. *Faraday Soc.* **1961**, *57*, 1603–1611.

48. Benck, J. D.; Hellstern, T.R.; Kibsgaard, J.; Chakthranont, P.; Jaramillo, T. F. Catalyzing the Hydrogen Evolution Reaction (HER) with Molybdenum Sulfide Nanomaterials. *ACS Catal.* **2014**, *4*, 3957–3971.
49. Tsai, C.; Chan, K.; Abild-Pedersen, F.; Nørskov, J. K. Active Edge Sites in $MoSe_2$ and WSe_2 Catalysts for the Hydrogen Evolution Reaction: a Density Functional Study. *Phys. Chem. Chem. Phys.* **2014**, *16*, 13156–13164.
50. Parsons, R. The Rate of Electrolytic Hydrogen Evolution and the Heat of Adsorption of Hydrogen. *Trans. Faraday Soc.* **1958**, *54*, 1053–1063.
51. Trasatti, S. Work Function, Electronegativity, and Electrochemical Behaviour of Metals: II. Potentials of Zero Charge and "Electrochemical" Work Functions. *J. Electroanal. Chem.* **1971**, *33*, 351–378.
52. Geeley, J.; Jaramillo, T. F.; Bonde, J. L.; Chorkendorff, I.; Nørskov, J. K. Computational High-Throughput Screening of Electrocatalytic Materials for Hydrogen Evolution. *Nat. Mater.* **2006**, *5*, 909–913.
53. Jaramillo, T. F.; Jørgensen, K. P.; Bonde, J.; Nielsen, J. H.; Horch, S.; Chorkendorff, I. Identification of Active Edge Sites for Electrochemical H_2 Evolution from MoS_2 Nanocatalysts. *Science* **2007**, *317*, 100–102.
54. Bonde, J.; Moses, P. G.; Jaramillo, T. F.; Nørskov, J. K.; Chorkendorff, I. Hydrogen Evolution on Nano-Particulate Transition Metal Sulfides. *Faraday Discuss.* **2008**, *140*, 219–231.
55. Kautek, W.; Gerischer, H. Anisotropic Photocorrosion of n-Type MoS_2 $MoSe_2$, and WSe_2 Single Crystal Surfaces: the Role of Cleavage Steps, Line and Screw Dislocations. *Surf. Sci.* **1982**, *119*, 46–60.
56. Compton, R. G.; Banks, C. E. *Understanding Voltammetry*; World Scientific Publishing Co. Pte. Ltd.: Singapore, 2007.
57. Konopka, S. J.; McDuffie, B. Diffusion Coefficients of Ferri- and Ferrocyanide Ions in Aqueous Media, Using Twin-Electrode Thin-Layer Electrochemistry. *Anal. Chem.* **1970**, *42*, 1741–1746.
58. Hoang, S.; Guo, S.; Hahn, N. T.; Bard, A. J.; Mullins, C. B. Visible Light Driven Photoelectrochemical Water Oxidation on Nitrogen-Modified TiO_2 Nanowires. *Nano Lett.* **2012**, *12*, 26–32.